

Pattern formation of granules on the bottom of a differentially rotating tank

By P. J. THOMAS

Department of Applied Mathematics and Theoretical Physics, University of Cambridge,
Silver Street, Cambridge, CB3 9EW, UK

(Received 7 October 1993 and in revised form 11 March 1994)

The formation of patterns of granules on the bottom of a differentially rotating tank, partially filled with a fluid, is described. The pattern formation is initiated when the tank is spun up from an initial constant rotation rate by a sufficiently large increment to another constant higher rotation rate. The granules are observed to be set into motion, slide across the bottom of the tank and organize themselves into two distinct, superposed geometrical patterns. The first pattern constitutes a system of tightly wound equi-angular spirals and is identified as being simply a visualization of the well-known stationary Class B waves of the unstable boundary layer. This pattern is not considered further here. The second pattern, which is considered here, is shown not to be a visualization of some other known stationary wave mode. It consists of a number of large-scale spiral arms extending outward towards the wall of the tank and originating at a patch of salt in the tank's centre. The presence of Class B waves is apparently a necessary condition for the spiral arm formation. The experiments show that the radius r_0 of the inner salt patch is inversely proportional to the increment $\Delta\omega$ of the rotation rate for the larger values of $\Delta\omega$. The angle $\epsilon(r)$ between the direction of the spiral arms and the tangential direction is observed to decrease with the distance r from the centre as r^b where $b = -0.64 \pm 0.1$. The relationship between the number n of spiral arms and the associated Reynolds number Re and Rossby number Ro is found from the experimental observations and dimensional considerations to be

$$n^2 = Re Ro.$$

Various aspects related to the mechanism involved in the pattern formation are discussed. However, no conclusive model for the spiral arm formation can at present be suggested.

1. Introduction

The present paper describes the formation of patterns of granules on the bottom of a differentially rotating tank which is partially filled with a fluid. It will be seen that the formation of the observed patterns arises in close association with the instability of the laminar Ekman boundary layer on the bottom of the tank. This introduction will thus first summarize the relevant literature concerning the stability of the boundary layer on a rotating disk.

Since Faller (1963) and Tatro & Mollö-Christensen (1967) presented their results, it has been established that the laminar Ekman layer on a rotating disk or on the bottom of a rotating tank may exhibit at least two different types of instability (see also Faller & Kaylor 1966, 1967; Caldwell & Van Atta 1970). These two types of instability are

often referred to as Class A (or Type II) and Class B (or Type I) instability waves in the literature. The wavelength of both classes of instabilities depends on the characteristic depth of the boundary layer on the bottom of the tank which is given approximately by the Ekman thickness δ

$$\delta = (\nu/\omega)^{0.5}, \quad (1)$$

where ν is the viscosity of the fluid and ω is the basic rotation rate. The wavelength λ_A of the Class A waves is around

$$\lambda_A \approx 28 \delta \quad (2)$$

and the Class B waves have a somewhat shorter wavelength λ_B of approximately

$$\lambda_B \approx 11.8 \delta \quad (3)$$

(see for instance Greenspan 1968).

The phase speed of the Class A and the Class B waves is directed radially inward and takes values of approximately 0.16 and 0.034 times the azimuthal component of the interior flow velocity respectively. The Class A waves are orientated at an angle ϵ of between $+5^\circ$ (to the left) and -20° (to the right), with respect to the tangential flow direction. The angle ϵ for the Class B waves is observed to be approximately $+15^\circ$. Both classes of instability form systems of horizontal roll vortices within the boundary layer. Tatro & Mollö-Christensen (1967) report that the Class A waves occur at a lower critical Reynolds number and are very sensitive to the Rossby number. The Class B waves occur at a higher critical Reynolds number and reveal only a slight Rossby-number dependence. Stationary Class B waves modes were first observed by Gregory, Stuart & Walker (1955). They used the china-clay technique to visualize the presence of instability on a rotating disk in free air where the Class B waves produce weak marks spiralling outwards around the centre of the disk. Faller & Kaylor (1965) (cited in Tatro & Mollö-Christensen 1967) first observed the Class A waves.

Since these early investigations the instability of the boundary layer on a rotating disk has been the focus of numerous studies and a summary of the available literature has recently been published by Reed & Saric (1989). Only stationary wave modes and possibly modes with very low phase speeds can be visualized by techniques involving granules. Hence, it is only those waves that appear relevant in the context of the present experiment. Stationary Class B waves were, for instance, studied by Federov *et al.* (1976), Kobayashi, Kohama & Takamadate (1980), Malik, Wilkinson & Orszag (1981) and Kohama (1984). Values of the critical Reynolds number for the onset of instability of between 280 and 530 have been reported by various authors, with the Reynolds number being defined as $(r^2\omega/\nu)^{0.5}$, where r is the local radius, ω is the rotation rate and ν is the kinematic viscosity. The number of vortices observed in all these studies is around 32. However, Federov *et al.* (1976), who reported experiments employing naphthalene sublimation and acoustic techniques, found 14–16 vortices propagating at an angle of $\epsilon = 20^\circ$ at a lower Reynolds number of 245. It is believed that the somewhat different results reported by various authors are largely due to differences in surface roughness of the disks and the detection techniques employed (see for instance Wilkinson & Malik 1985). Kohama (1984, 1987) additionally reported the observation of ring-like vortices on the surface of each of the spiral vortices discussed above. These ring-like vortices are described as initially looking like waves and then developing into corotating vortices as they travel along the spiral vortex.

The purpose of this paper is to document and discuss the results obtained for a set of runs of an experiment which involves the observation of the formation of patterns

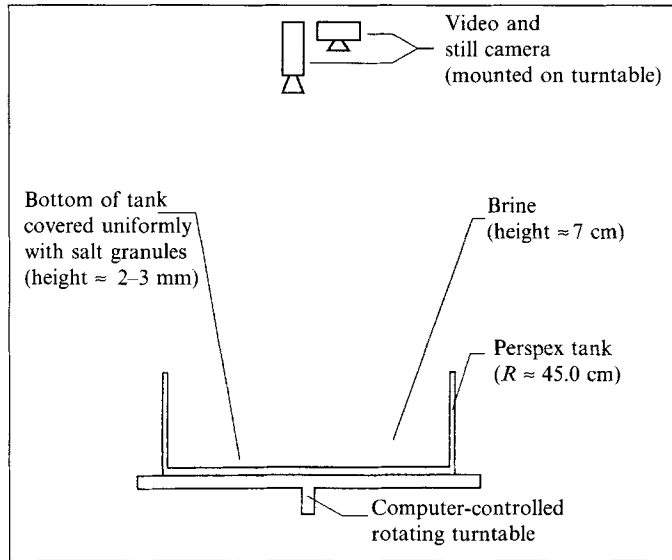


FIGURE 1. Sketch of the experimental set-up.

of granules on the bottom of a differentially rotating tank which is partially filled with a fluid. Whereas the formation of these patterns will be found to arise in close association with the above discussed instability of the boundary layer it will, however, be seen that the patterns discussed here are not simply a visualization of some previously known stationary wave mode.

2. Experimental set-up

The experiments described below were carried out in a circular Perspex tank with a radius $R \approx 45$ cm positioned on a computer-controlled turntable (see figure 1). The tank was filled to a height of approximately 7 cm with a supersaturated brine solution such that no additional salt could be dissolved in the fluid. The temperature of the brine was constant for all runs of the experiment at approximately 20 °C and the density ρ_f of the brine was determined as $\rho_f = 1.2055 \text{ g cm}^{-3}$. Further salt was added to the tank until the bottom of the tank was covered uniformly with a layer of salt approximately 2–3 mm thick. The turntable was then gradually sped up to a terminal rotation rate ω_0 of up to about 3.0 rad s^{-1} in such a way that the salt on the bottom of the tank was not disturbed by the relative motion between the accelerating tank and the spinning-up fluid lagging behind. Once the system had reached its terminal rotation rate ω_0 and after all fluid motion inside the tank had died away the turntable was accelerated further by an increment $\Delta\omega$ to a rotation rate ω_1 . The increment $\Delta\omega$ was as large as 3.5 rad s^{-1} and the acceleration $d\omega/dt \approx 0.1 \text{ rad s}^{-2}$ during the acceleration phase was the same for all runs of the experiment. When the increment $\Delta\omega$ was large enough to cause the salt particles on the bottom of the tank to be set into motion, they were observed to organize themselves to show two distinct geometrical patterns superposed on each other.

Flow visualization was achieved with a video and a still camera mounted in the rotating frame of reference on the turntable above the centre of the tank with both the cameras pointing perpendicularly downwards. The bottom of the tank was black so

that the process of the pattern formation of the white salt granules became visible against the dark background.

3. Experimental results

3.1. Description of the developing patterns

A reorganization of the salt granules together with a pattern formation was observed to occur whenever the increment $\Delta\omega$ of the rotation rate of the turntable was large enough to cause those salt particles initially located at radii greater than some critical radius to be set into motion and slide across the bottom of the tank towards its wall. The structure observed to develop consists of two distinct patterns superposed on each other. These two patterns are first a pattern of marks in the salt bed consisting of tightly wound equi-angular spirals, spiralling outwards around the centre of the tank and starting at some radius away from the tank's centre. This first pattern will be referred to as the small-scale pattern or the small-scale spirals (shown in figure 2*d* below). The second pattern forming is one on which the small-scale pattern is superposed. This second pattern consists of a number n of spiral arms extending outward towards the wall of the tank originating from a uniform salt patch with a radius r_0 in the tank's centre which apparently remains unaffected by the ongoing reorganization process. This second pattern will be referred to as the large-scale pattern or the (large-scale) spiral arms. The number n of these spiral arms observed in the present experiment ranged from as few as 7 to as many as approximately 110. We define the wavelength $\lambda(r)$ of the spiral arms as the azimuthal spacing between the centres of two neighbouring spiral arms given by

$$\lambda(r) = 2\pi r/n \quad (4)$$

for any $r_0 < r \lesssim R$. Typical examples of the developing patterns are shown in figure 2(*a-d*). Figure 2(*a*) shows a spiral pattern during its formation phase and figures 2(*b-d*) were captured after the completion of the reorganization process for different runs of the experiment. Lengthscales on the pictures can be inferred from the reference circles visible through the transparent bottom of the Perspex tank. The radial distance between two such adjacent circles is 5 cm and the visible numbers on the reference background indicate the distance in cm from the centre of the tank. The pattern formation process in the experiment for all runs appeared to be concluded within several seconds after the turntable had reached its final rotation rate ω_1 . Once a pattern had formed it remained apparently stationary, i.e. there was no noticeable motion of the pattern with respect to the bottom of the tank. However, for the runs of the experiment with the highest values of the rotation rate ω_1 and large increment $\Delta\omega$ it was observed that the large-scale pattern seemed to fade somewhat while not changing its shape if the run was continued for several minutes after the spiral arms were initially formed. This shows clearly that, at least in these cases, there was still some granule motion even after the apparently stationary pattern was formed. Close-up recordings of such runs of the experiment have shown that this granule motion takes place along the boundary of the spiral arms. However, in this paper we are concerned with the global geometrical properties of the developing patterns and will thus not consider this any further.

Figure 2(*a*) shows that the spiral arms are apparently formed first in the more central portion of the tank, while the salt granules further away from the centre are still in motion. The video recordings indicate that the paths followed by the individual granules apparently do not necessarily coincide with either the direction of the spiral arms or with the direction of the small-scale spirals. This leads, during the formation

process of the spiral arms, to some granule exchange between neighbouring spiral arms, with the direction of this exchange being determined by the large-scale fluid flow relative to the table. The somewhat larger white dots visible on figure 2(a) are small pieces of paper floating on the surface of the water; these were added during some runs of the experiment to visualize the fluid motion with respect to the turntable. After the completion of the formation process the large-scale spiral arms are easily identified on each of figures 2(b)–(d) displaying $n \approx 25, 51, 63$ arms respectively, with different radii of the inner salt patch. The spiralling angle ϵ between the direction of the spiral arms and the tangential direction can be seen in figure 2(b) to decrease with increasing distance r from the centre of the tank.

In contrast to the large-scale spiral arms, the small-scale pattern which was present in all runs of the experiment can only be seen satisfactorily in figure 2(d) where it can be identified as very weak light and dark equidistant outward-spiralling streaks superposed on the outermost region of the inner salt patch and the large-scale spiral arms. Figure 2(d) shows that for locations not too far radially outwards from the inner salt patch, where the spacing between two adjacent large-scale arms is not yet too large, the small-scale structure tends to form bridges between two neighbouring large-scale spiral arms, connecting them. Note that care has to be taken not to confuse these bridges with segments of the reference circles on the bottom of the tank.

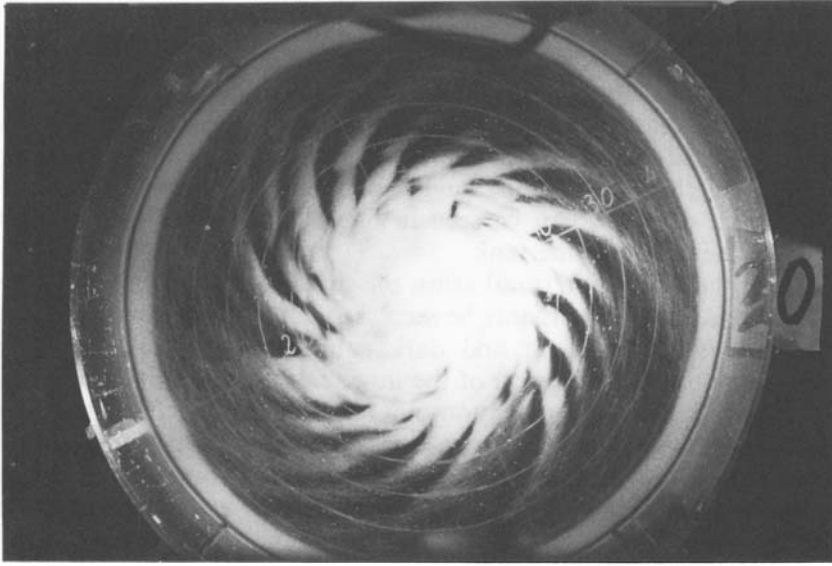
An attempt was made to render more clear the difference between the large-scale and the small-scale patterns and to obtain additional information on the flow along the bottom of the tank by adapting the suggestion made by one of the referees to carry out some additional runs of the experiment employing a dye-visualization technique. For these runs a number of potassium permanganate granules were dropped on the surface of the salt layer on the bottom of the tank prior to accelerating the turntable from ω_0 to ω_1 . However, this approach did not lead to any improvement in the representation of the pattern structure in the present experiment nor did it yield any additional results concerning the flow structure on the bottom of the tank. From these additional runs it was, moreover, not possible to arrive at a more detailed account of the paths taken by the individual granules during the reorganization process.

3.2. Parameter regime of pattern formation

The diagram of figure 3 shows the regime where a successful large-scale pattern formation was observed, with each data point representing one successful run of the experiment. A run of the experiment is referred to as successful whenever a clear large-scale pattern developed such that the number of large-scale spiral arms could be counted. Thus, there is no sharp boundary between the regime of successful pattern formation and the regime of no pattern formation as will become more clear from the discussion of figure 3. The abscissa in figure 3 represents the rotation rate ω_0 from which the tank was accelerated by an increment $\Delta\omega$ to the rotation rate ω_1 . The dotted line in figure 3 separates the two regimes of successful pattern formation and no pattern formation. As the highest possible rotation rate ω_1 for the present experiments was 3.5 rad s^{-1} , no data points are available in the upper right area of the diagram. Nevertheless, with regard to the available data, a successful pattern formation is probable at least for the majority of combinations of ω_0 and $\Delta\omega$ of this region. The experiments have shown that for spin-up from rest the onset of the large-scale spiral arm formation is first observed for values for ω_1 of $\omega_1 \gtrsim 1.0 \text{ rad s}^{-1}$ with a distinct pattern developing for values of $\omega_1 \gtrsim 1.5 \text{ rad s}^{-1}$. The critical threshold value $\Delta\omega_c = \omega_c$ necessary for a successful pattern formation is thus taken as

$$\Delta\omega_c = \omega_c = 1.0 \text{ rad s}^{-1}. \quad (5)$$

(a)



(b)

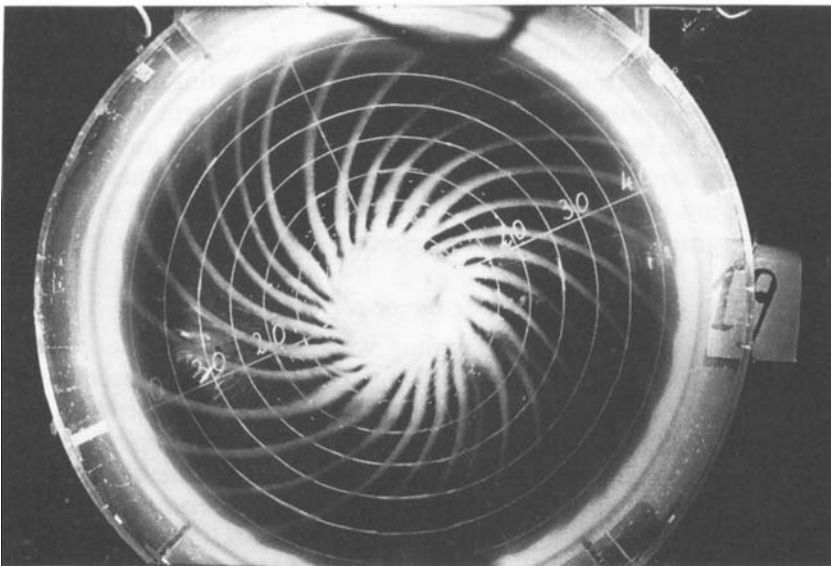


FIGURE 2(*a, b*). For caption see facing page.

From figure 3 it can, moreover, be seen that for increasing ω_0 the critical value of $\Delta\omega$ which is required for a successful pattern formation decreases to a value of around $\Delta\omega \approx 0.2\text{--}0.3 \text{ rad s}^{-1}$ for $\omega_0 = 3.0 \text{ rad s}^{-1}$. The decrease appears to reflect the combined effect of the sum of the main forces acting on the salt granules due to shear stresses and the centrifugal force while they are still resting on the salt bed on the bottom of the tank. A trivial but necessary condition for successful pattern formation is, obviously,

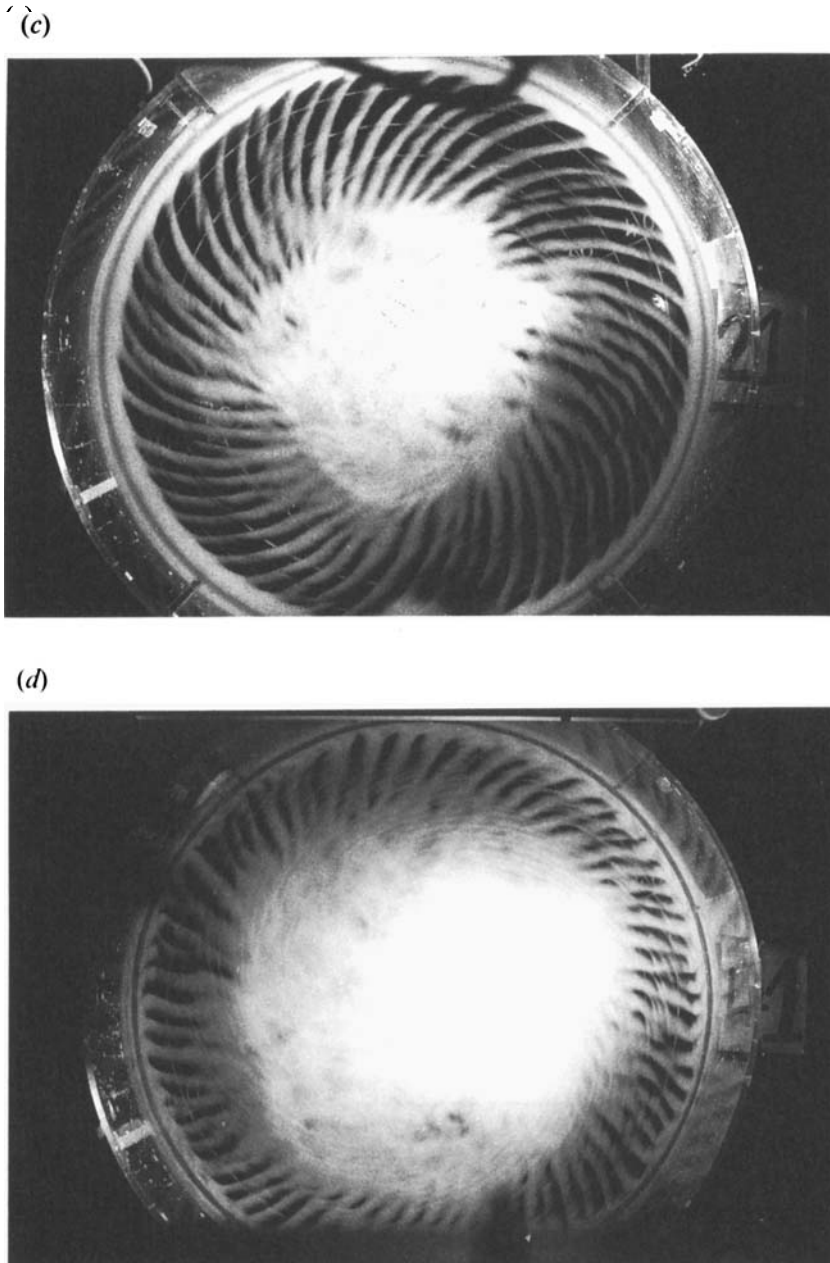


FIGURE 2. Developing patterns of the salt granules (the sense of rotation of the turntable is anticlockwise): (a) during formation process; (b–d), after completion of pattern formation. (a) $\Delta\omega = 1.9 \text{ rad s}^{-1}$, $\omega_1 = 2.1 \text{ rad s}^{-1}$; (b) $\Delta\omega = 1.6 \text{ rad s}^{-1}$, $\omega_1 = 3.4 \text{ rad s}^{-1}$; (c) $\Delta\omega = 0.8 \text{ rad s}^{-1}$, $\omega_1 = 3.1 \text{ rad s}^{-1}$; (d) $\Delta\omega = 0.6 \text{ rad s}^{-1}$, $\omega_1 = 2.4 \text{ rad s}^{-1}$. (The small-scale spiral pattern can be identified in (d) as very weak light and dark equidistant outward-spiralling streaks superposed on the outermost region of the inner salt patch and the large-scale spiral arms.)

that motion of the granules has to be initiated. The magnitude of the shear stresses depends on $\Delta\omega$ whereas the centrifugal force acting on the granules increases with an increasing absolute value of the rotation rate of the turntable. Hence, the critical value of the increment $\Delta\omega$ of the rotation rate necessary for the initiation of granule motion

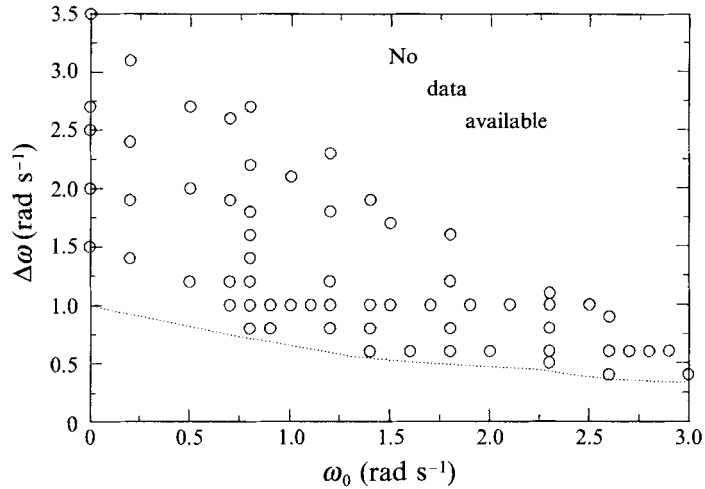


FIGURE 3. Diagram of successful pattern formation. The data points indicate the runs of the experiment where the increment $\Delta\omega$ leads to pattern formation when the tank is spun up from the rotation rate ω_0 .

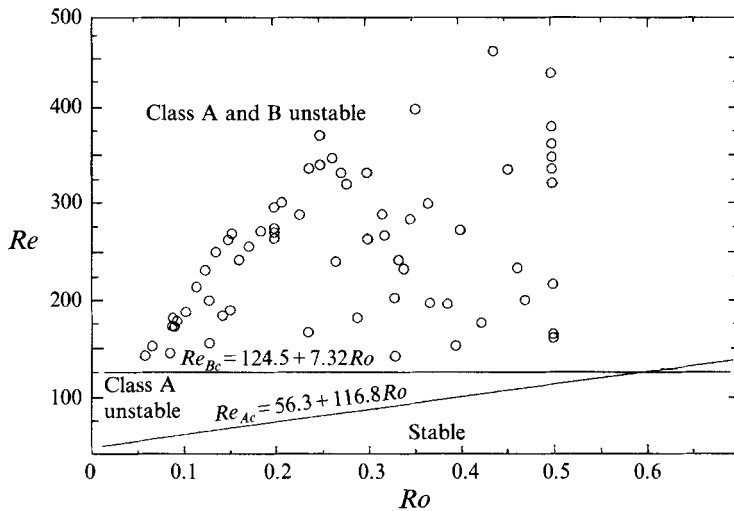


FIGURE 4. Data points for the successful runs of the present experiment where a pattern formation was observed in comparison to the stability diagram of Tatro & Mollö-Christensen (1967) for the Class A and the Class B waves. Their definitions of Reynolds and Rossby numbers are used: $Re = \Delta\omega r_0 \delta / \nu$, $Ro = \Delta\omega r_0 / (2\omega_1 r_0)$, $\delta = 2.58(\nu/\omega_1)^{0.5}$.

and thus successful pattern formation must decrease with an increasing absolute rotation rate ω_1 of the turntable, as it was observed in figure 3.

The small-scale pattern identified in figure 2(d) is strongly reminiscent of the spiral pattern expected to be created by the roll vortices pertaining to the Class B waves of the boundary-layer instability (compare for instance with the photos in Gregory *et al.* 1955 or Faller 1963). From figure 2(d) it can be estimated that the constant distance between the adjacent crests of two such neighbouring spirals is of the order of 1 cm, which is a typical value for all runs of the experiment. This value is consistent with the

prediction obtained from equation (3) for the wavelength λ_B of Class B waves which is, for $\omega = \omega_1$ and values of ω_1 between approximately 1.5 and 3.5 rad s⁻¹, expected to be in the range of approximately 0.8 and 1.3 cm. The spiralling angle ϵ formed by the light and dark streaks seen in figure 2(d) with respect to the tangential direction can be measured from the photos as approximately 15°. This is the angle expected for Class B waves. It can thus be concluded that the small-scale pattern is merely a visualization of the stationary Class B waves in the boundary layer. This pattern will not be considered further in this paper.

The wavelength $\lambda(r)$ of the large-scale spiral arms observed here is proportional to the radial position r whereas the wavelengths for Class A and Class B waves as given by (2) and (3) are expected to be approximately constant for varying r . Thus the large-scale spiral arms appear not to be simply a visualization of some other stationary wave mode of the discussed waves. It should be emphasized that the present large-scale spiral arms should not be confused with the vaguely similar looking structure of Faller's (1963) figure 3 in his original work. This structure is, in his case, merely an effect of the selective introduction of dye in the four sectors of his tank. (A reproduction of Faller's figure 3 can also be found in Greenspan 1968 as his figure 6.9.(a).)

Figure 4 shows the data points for the runs of the present experiment where a successful pattern formation was observed in comparison to the stability diagram obtained by Tatro & Mollö-Christensen (1967) for the onset of the occurrence of the Class A and the Class B waves. The lines marked with the expressions for Re_{Ac} and Re_{Bc} indicate the critical Reynolds numbers given by Tatro & Mollö-Christensen for the two wave classes as a function of the Rossby number. For figure 4 the definitions of the Reynolds number and the Rossby number for the present data points are those of Tatro & Mollö-Christensen and are indicated in the figure caption. Each data point in figure 4 corresponds to one successful run of the present experiment in which a large-scale spiral arm formation was observed. It can be seen that all the present data points lie above the stability boundary for the Class B waves, with this boundary approximately coinciding with the boundary of successful spiral arm formation. It can thus be concluded from figure 4 that the Class B waves are always present when a successful spiral arm formation is observed and that they, moreover, appear to be a necessary condition for the large-scale spiral arm formation. Hence, the experimental results indicate that the reorganization process of the salt granules and the instabilities supported by the boundary layer might be closely associated with each other with respect to the formation of the large-scale spiral arms.

None of the earlier researchers appear to have observed any indication of the formation of the large-scale spiral arms found in the present experiments. Moreover, no reference to a comparable process for the case of spin-down experiments could be found in the literature. While we have observed some pattern formation in the spin-down case this appears not to be as clear as the results described here for the spin-up case.

The spiral arms observed in the present experiment could obviously not be formed in Faller's experiment as he used a dye flow visualization technique rather than solid particles. Gregory *et al.*, however, did use solid particles, namely china clay, but did not observe any indication of the formation of the spiral arms. The discussion of the present results will show, however, that no such formation can be expected in their experiments.

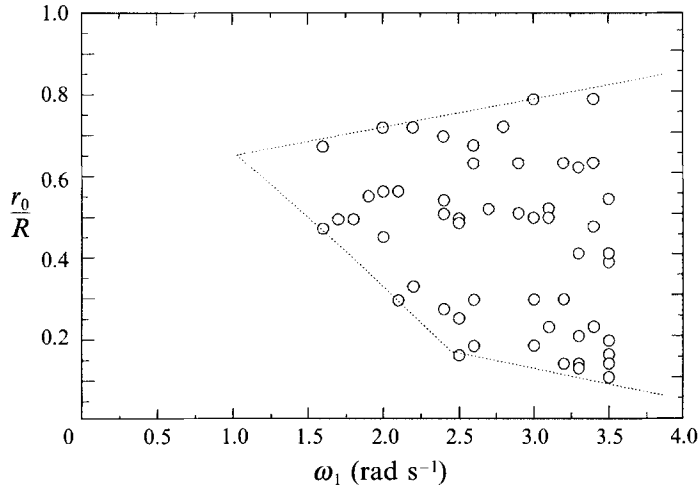


FIGURE 5. Dimensionless radius r_0/R of the inner salt patch for the runs of the experiment with successful pattern formation as a function of the absolute rotation rate ω_1 .

3.3. Experimental data for the spiral arm properties

As described above, the spiral arms developing during the runs of the experiment originate from a salt patch with a radius r_0 in the centre of the tank which apparently remains unaffected by the large-scale reorganization process. In the diagram of figure 5 the radius of this patch is plotted as a function of the absolute rotation rate ω_1 . The area in figure 5 surrounded by the dotted line and which includes the data points refers to the regime of successful pattern formation. In figure 5 the value of $\Delta\omega$ at any value of ω_1 decreases on traversing the regime of successful pattern formation vertically upwards. Hence the lower dotted line, representing the boundary of the regime, corresponds to the experiments in which the tank was spun up from rest. The upper boundary corresponds to the smallest value of $\Delta\omega$ at which, for a given ω_1 , successful pattern formation can be expected. The lower and the upper boundary intersect at the point $\omega_1 \approx 1.0 \text{ rad s}^{-1}$, $r_0/R \approx 0.65$ which corresponds to the critical threshold value, identified in equation (5), below which pattern formation is not possible at all. Figure 5 does not reveal any systematic dependency of the radius of the inner patch on the absolute rotation rate ω_1 . For any given ω_1 above the critical threshold value $\omega_c \approx 1.0 \text{ rad s}^{-1}$ a set of solutions for the radius of the patch is possible which appears only to be bounded by an upper and a lower limit. The upper limit of the patch radius increases with increasing rotation rate ω_1 and the lower limit of the patch radius decreases with increasing ω_1 . This result can again be explained qualitatively by considering the combined action of the sum of the main forces acting on the salt granules while they are still at rest on the bottom of the tank. The lower boundary of the regime of successful pattern formation in figure 5 corresponds to large values of $\Delta\omega$, i.e. spin-up from rest and large shear stresses; the upper boundary corresponds to low values of $\Delta\omega$ and thus small shear stresses. Hence, along the lower boundary an increase of ω_1 leads to the motion of salt granules at locations increasingly closer to the centre of the tank. Along the upper boundary the force due to shear stresses is generally smallest; but as larger values of $\Delta\omega$ are required for small ω_1 to initiate any granule motion, the radius of the inner patch is effectively increased with increasing ω_1 .

A remark concerning the possible influences of the height of the fluid layer in the tank on the pattern formation process should be included at this point. The pattern

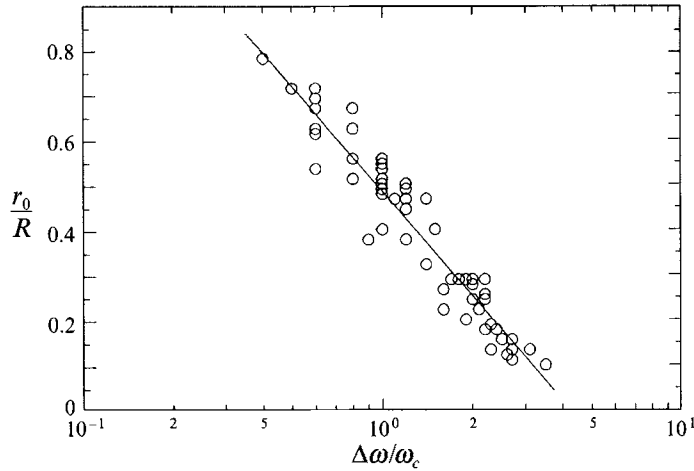


FIGURE 6. Dimensionless radius r_0/R of the inner salt patch for the runs of the experiment with successful pattern formation as a function of the dimensionless increment $\Delta\omega/\omega_c$ of the rotation rate. The line represents the least-squares fit to the data points which is given by $r_0/R \approx -0.340 \ln(\Delta\omega/\omega_c) + 0.487$; $\omega_c \approx 1.0 \text{ rad s}^{-1}$, $R = 44.75 \text{ cm}$.

formation process of the salt granules takes place in the region of the boundary layer on the bottom of the tank. The shear stresses generated in the boundary layer, which act on the granules, must be one of the main initiation and driving mechanisms of the formation process. It can be assumed that the fluid layer height will not have any significant influence on the pattern formation process as long as it is large compared with the height δ (given by (1)) of the boundary layer on the bottom of the tank. This condition is satisfied for all runs of the present experiment.

Figure 6 shows the dependence of the radius r_0/R of the inner salt patch on the increment $\Delta\omega/\omega_c$ of the rotation rate. The error involved in determining the radius of the salt patch from the video recordings is estimated to be of the order of $\pm 0.05 r_0/R$. It can be seen that the data points are best represented by the expression

$$r_0/R = -0.340 \ln(\Delta\omega/\omega_c) + 0.487. \quad (6)$$

If the data of figure 6 were alternatively plotted in a double logarithmic representation it would be seen that the data points for $\Delta\omega/\omega_c \gtrsim 1.0$ can be fitted by the power law relationship

$$r_0/R = 0.5(\Delta\omega/\omega_c)^{-1.05}. \quad (7)$$

Nevertheless, this would require neglecting around 25% to 30% of all the available data for which $\Delta\omega/\omega_c \lesssim 1.0$ and for which the patch radius is overestimated by this power law relationship. The exponent of approximately -1 in the power law is the result one would expect when the force required to lift the granules from the salt bed is constant and the centrifugal force can be neglected. On the basis of the results obtained for the present experiment it is, however, not possible to decide whether the deviation from the power law relationship for $\Delta\omega/\omega_c \lesssim 1.0$ has to be attributed to the increasing importance of the centrifugal force for small values of $\Delta\omega$ or possibly to the finite size of the tank.

It was observed in figure 2 that the spiralling angle ϵ of the large-scale spiral arms decreases with increasing radial distance r from the tank's centre. For the different runs of the experiment, values for ϵ of between $\epsilon \approx 80^\circ$ near the inner salt patch and $\epsilon \approx 30^\circ$ at the outermost positions of the spiral arms were observed. Figure 7 shows the data

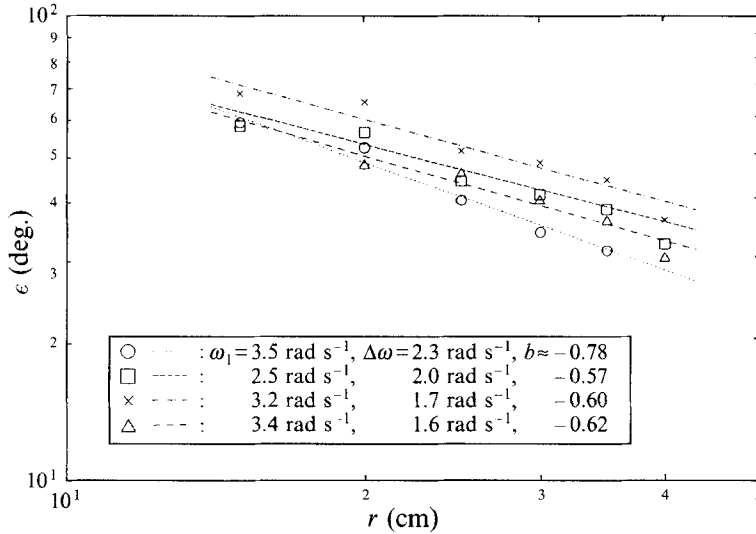


FIGURE 7. Spiralling angle ϵ as a function of the distance r from the tank's centre, for four different runs of the experiment.

obtained for the angle ϵ as a function of the radial position r for four different runs. The data clearly reveal a relationship between the two parameters as $\epsilon \propto r^b$. A mean value for the exponent b was determined as $b = -0.64 \pm 0.10$ from all the evaluated photos. This mean value, however, has to be viewed with some care. A reliable data set for $\epsilon(r)$, with a sufficient number of data points, can only be obtained if the inner salt patch is not too large in comparison with the radius R of the tank. The data evaluation will thus necessarily have to favour the results obtained for ϵ from those runs of the experiment with parameter configurations leading to a small inner salt patch. This will mask possible dependencies of the exponent b on the increment $\Delta\omega$ of the rotation rate and on the absolute rotation rate ω_1 . Owing to the restricted tank size the available data are, however, not sufficient to establish such possible dependencies unambiguously. It should furthermore be noted here that it is conceivable that the dependency found for the spiralling angle $\epsilon(r)$ might additionally be biased to some extent by end-wall effects due to the finite size of the tank. However, in order to investigate this possibility a number of large tanks with different radii is required; such different sized tanks were unfortunately not available to us. Nevertheless, as one would expect, figure 7 does at least appear to reveal a trend for the angle ϵ to decrease with an increasing increment of the rotation rate $\Delta\omega$ for the displayed data of the three runs which have approximately equal values of the absolute rotation rate ω_1 with $\omega_1 > 3.0 \text{ rad s}^{-1}$.

We will now consider the experimental results for the number of spiral arms that develop. Figure 8 shows the dependency of the number n of spiral arms on the absolute rotation rate ω_1 , obtained for two different values of the increment $\Delta\omega$. It can be seen that a least-squares fit to the data points reveals a power law dependence of n on the absolute rotation rate ω_1 as

$$n \propto \omega_1^{0.5} \quad (8a)$$

or with (4)

$$\lambda(r) \propto \omega_1^{-0.5} \quad (8b)$$

for any $r = \text{const}$ with $r_0 < r \lesssim R$. A comparison with (1), (2) and (3) suggests that this result might reflect the influence of the boundary-layer instability on the reorganization process and thus on the large-scale spiral arm formation.

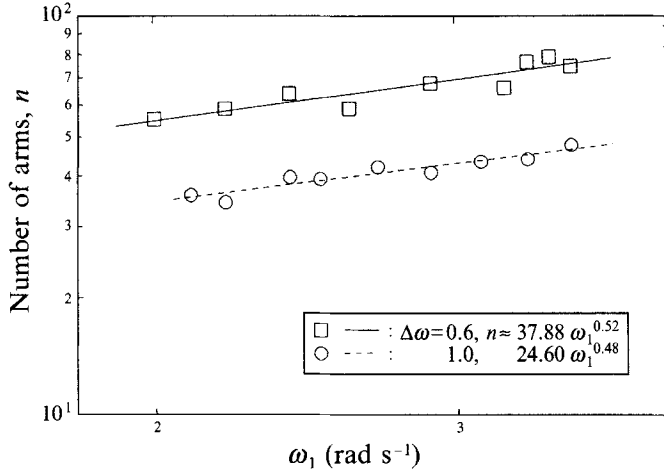


FIGURE 8. The number n of large-scale spiral arms as a function of the absolute rotation rate ω_1 , for two different increments $\Delta\omega$ of the rotation rate.

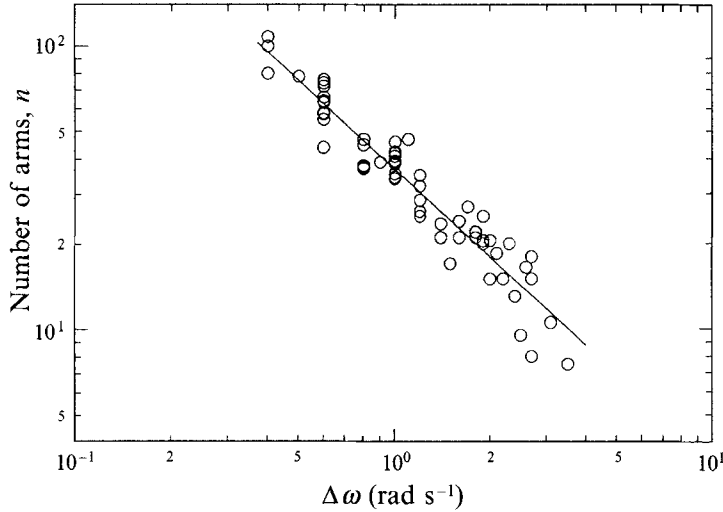


FIGURE 9. The number n of large-scale spiral arms as a function of the increment $\Delta\omega$ of the rotation rate. The line represents the least-squares fit to the data points which is given by $n = 36.80\Delta\omega^{-1.04}$.

However, the number n of spiral arms also depends on the increment $\Delta\omega$ of the rotation rate and this dependence is displayed in figure 9. A least-squares fit to the data points, which is equivalent to averaging out the influence of the absolute rotation rate ω_1 shows that

$$n \propto \Delta\omega^{-1}. \tag{9}$$

When both the above results are combined it is seen from figure 10 that all data points for the number n of spiral arms collapse onto one straight line in double logarithmic representation when plotted as a function of $\omega_1^{0.5}/\Delta\omega$, with the least-squares fit to the data points being given by

$$n = c(\omega_1^{0.5}/\Delta\omega)^{0.96} \tag{10}$$

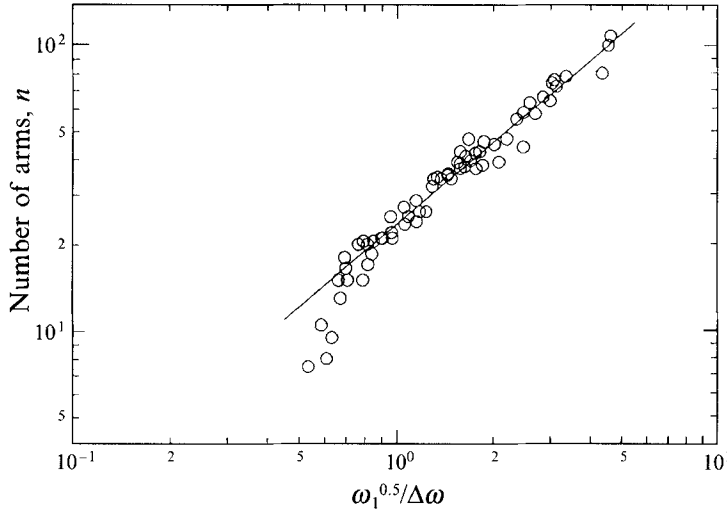


FIGURE 10. The number n of large-scale spiral arms as a function of $\omega_1^{0.5}/\Delta\omega$. The line represents the least-squares fit to the data points which is given by $n = 23.53 (\omega_1^{0.5}/\Delta\omega)^{0.96}$.

and a numerical value of the constant c of $c \approx 23.53$. The exponent obtained from the least-squares fit is sufficiently close to 1 to conclude that

$$n = c \omega_1^{0.5}/\Delta\omega \quad (11)$$

which is the final empirical result. In order to assure the dimensional consistency of equation (11) the constant c must be required to have the dimension $s^{-0.5}$. Some deviation from the relationship (11) is observed for the data points with low values for n of $n \lesssim 10$ which correspond to those runs of the experiment with large values of $\Delta\omega$ and small values of ω_0 (i.e. spin-up from rest to high rotation rates).

4. Discussion of the experimental data for the number of spiral arms

In the preceding section the numerical value obtained from the least-squares fit for the constant c in (10) was not dimensionally correct. It was argued, however, that this constant must have the dimension $s^{-0.5}$ to assure the dimensional consistency of the final result, equation (11), for the number of spiral arms. In the following dimensional consideration the constant c will now be discussed in greater detail.

It can be assumed that the number n of the spiral arms developing depends on the reduced gravitational acceleration g' which is defined as

$$g' = g(\rho_g - \rho_f)/\rho_g, \quad (12)$$

where ρ_g and ρ_f are the densities of the granules and the fluid respectively and g is the gravitational acceleration. If the constant roughness of the floor is neglected the only further parameters entering the problem are the granule diameter d_p (since the large-scale spiral arms result from the motion of the granules on the bottom of the tank) and finally the viscosity ν of the fluid. Using the experimental result of equation (11) that the number of spiral arms n is proportional to $\omega_1^{0.5}/\Delta\omega$ a dimensional consideration then shows that the governing dimensionless parameter k , inherent in the problem of determining the number of spiral arms that develop, must be given by

$$k = g' d_p \omega_1 / (\nu \Delta\omega^2). \quad (13)$$

A comparison of (11) and (13) now yields the result that

$$n^2 = k \quad (14a)$$

with the constant c of (11) being written as

$$c = (g'd_p/\nu)^{0.5} \quad [\text{s}^{-0.5}]. \quad (14b)$$

When one replaces ω_1 in (13) with the help of the relation $v(r) = \omega_1 r$, a Reynolds number Re and a Rossby number Ro characterizing the system can be defined as

$$Re = d_p v(r)/\nu \quad (15a)$$

and
$$Ro = \frac{g'/\Delta\omega}{\Delta\omega r} \quad (15b)$$

and one finds that (14a) can be formally rewritten as

$$n^2 = Re Ro \quad (16)$$

as the final result.

This is a remarkably simple relationship considering the apparent complexity of the granule motion and the granule interaction with the instability of the boundary layer on the bottom of the tank. If a variable roughness of the floor is allowed for, a further lengthscale, characterizing the roughness depth of the bottom of the tank, enters the problem and the above result will have to be modified accordingly by introducing a further dimensionless parameter.

During the experiments the density of the brine was measured as $\rho_f = 1.2055 \text{ g cm}^{-3}$; with this the particle diameter d_p of the salt granules effectively remains the only unknown quantity of the problem. As a plausibility check for the correctness of the result of (14) it is possible to obtain an estimate of the particle diameter as follows. From the density measurement one can conclude that the amount of salt dissolved in one litre of the fluid in the tank is approximately 310 g l^{-1} . The viscosity ν of the brine at room temperature then takes a value of around $\nu \approx 0.017 \text{ cm}^2 \text{ s}^{-1}$ (see for instance Weast 1971). From the data of the density measurement and the amount of salt dissolved in one litre of the brine one can infer the density of the salt and hence the granules as approximately $\rho_g \approx 1.8 \text{ g cm}^{-3}$. This yields for the reduced gravitational acceleration g' a value of $g' \approx 324 \text{ cm s}^{-2}$. From this, (14b) and the numerical value for c obtained from the least-squares fit (see (10)) one finds $d_p \approx 0.3 \text{ mm}$ for the granule diameter.

This estimate for the granule size was verified experimentally by examining a sample of salt granules contained in a supersaturated salt solution under a Leitz, Laborlux K microscope fitted with a graticule ($100 \times 0.01 \text{ mm} = 1 \text{ mm}$) at a magnification of 100. The salt granules were observed to have an almost quadratic cross-section with their edges somewhat rounded off. The majority of granules were observed to have an edge length between approximately 0.2 and 0.4 mm. Additionally, the size distribution of a sample of 1 kg of salt granules was determined by means of an Endecotts, Octagon 200 Test Sieve Shaker. This size analysis has shown that the average granule diameter is approximately between 0.29 and 0.32 mm with the diameter of around 75% of all granules lying within the size interval of 0.2 and 0.4 mm. This experimentally obtained result for the granule size is in very good agreement with the estimate obtained above and it thus supports the relation (14) for the number of spiral arms and the form of the constant c .

The result (14) moreover correctly predicts that no large-scale pattern formation can be expected for the experiments of Gregory *et al.* cited above. Using the relevant

numerical values for their experiments, i.e. $g' = g \approx 981 \text{ cm s}^{-2}$, the viscosity of air $\nu \approx 0.151 \text{ cm}^2 \text{ s}^{-1}$, a granule diameter of the china clay of the order of $d_p \approx 0.01\text{--}0.001 \text{ cm}$ or less, and taking $\Delta\omega = \omega_1$ (spin-up from rest) for rotation rates of $600\text{--}3200 \text{ rev min}^{-1}$ then (14) predicts values for the number n of spiral arms of the order of $n \lesssim 1\text{--}0.1$ or less.

Note that (14) states that a large-scale pattern formation in a particular fluid with one particular type of particle can only be expected to be observed in a certain range of values for the increment $\Delta\omega$ of the rotation rate and the absolute rotation rate ω_1 . For $\Delta\omega \rightarrow \omega_1$, i.e. spin-up from rest and with large values of ω_1 , as is the case for the experiments of Gregory *et al.*, one obtains $n \rightarrow 0$ as above. For the case of $\Delta\omega \rightarrow 0$ one obtains $n \rightarrow \infty$ for any ω_1 . With the condition that the number n of spiral arms is an integer and the wavelength $\lambda(r)$ given by (4), one then obtains $\lambda(r) \rightarrow 0$, again predicting that no pattern will be visible. The condition $\Delta\omega \neq 0$, which has to be viewed in relation to the onset of the boundary-layer instability, is a necessary condition for successful pattern formation. In other words, if the tank was somehow brought to a constant rotation rate at which the centrifugal force alone were sufficient to initiate particle motion, no pattern formation would be expected by the action of the centrifugal force and the Coriolis force alone. This result is supported by an experimental observation made for higher values of the absolute rotation rate ω_1 and not too large values of the increment $\Delta\omega$. During these runs of the experiment it was observed that a well-defined large-scale pattern was initially formed which apparently remained stationary for a short time and then after a delay of a couple of seconds started to blur. This blurring of the structure originates at the inner salt patch and spreads radially outwards until eventually the whole area between the inner salt patch and the wall of the tank is covered by a very thin, approximately uniform, and almost transparent sheet of salt. Note that the blurring is a different process than the fading of the spiral arms described during the discussion of figure 2.

An interesting observation in relation to ripple formation in a non-rotating system is obtained for constant rotation rates ω_1 . One finds from (14) and (4) that

$$\lambda(r) = \text{const.} \times r \Delta\omega, \quad (17)$$

or with $\Delta v(r) = \Delta\omega r$

$$\lambda(r) \propto \Delta v(r), \quad (18)$$

which is simply a consequence of the rotational geometry imposed on the system due to the rotational motion. Equation (18) is at odds with the result suggested by Owen (1980) for the wavelength of sand ripples in the case of ripple formation in a non-rotating system which is not restrained by symmetry conditions. Owen argues that in this case the wavelength of the ripples is proportional to the square of the wind velocity sustaining the formation process.

During the experiments, i.e. when the tank was spun up from ω_0 by an increment $\Delta\omega$ and pattern formation was initiated, it was occasionally observed that the developing large-scale pattern, especially for larger values of $\Delta\omega$, initially underwent a transformation process passing through a number of different pattern states with different numbers n of spiral arms before eventually settling for a terminal mode displaying a fixed number of arms. Simultaneously the curvature of the spiral arms was also observed to decrease and to approach a final less curved state. From the result of (13) and (14) that the number of spiral arms depends on $\Delta\omega$, the changing number n of spiral arms during the formation process has to be attributed to the finite interval of the acceleration period of the tank from the initial rotation rate ω_0 to the rotation rate ω_1 . The acceleration $d\omega/dt \approx 0.1 \text{ rad s}^{-2}$ of the tank was the same for all runs of

the experiment and hence the acceleration period for the largest values of $\Delta\omega$ was as long as approximately 30 s. In these cases, during the second half of this time interval, the reorganization process had already been initiated thus leaving the system in an undefined state for as long as up to about 15 s with respect to the number of developing spiral arms. This enables the developing pattern to progress through a number of different states before settling at its final mode. A consequence of this process is that in some instances it is observed that the stem of the spiral arms connecting these to the inner salt patch bifurcates into two spiral arms growing out of the same stem rather than just one well-defined spiral arm. This result adds some degree of ambiguity to the number n of arms counted during the data evaluation. Nevertheless, a preference for stem bifurcation is observed for small values of $\Delta\omega$ at high values of ω_1 where the number of developing spiral arms is large. Moreover, for none of these runs of the experiment was the number of bifurcated stems found to be higher than approximately five. In the case of an unequivocal stem bifurcation the two branching spiral arms were counted as one rather than two. It has to be emphasized then, that the finite acceleration period of the turntable in the present experiment does not have a significant influence on the final result and the developing mode displayed by the system as long as the interval of the acceleration is small compared to the time required by the system to reach the state of solid-body rotation. This was the case for all the runs of the present experiment.

5. Mechanism of the spiral arm formation, and conclusion

No mention has so far been made of the mechanism leading to the large-scale spiral arm formation. In this section some aspects of this mechanism will be briefly discussed.

One possible cause of the spiral arm formation that immediately springs to mind is some new set of roll vortices on the bottom of the tank with the axes of the vortices being orientated radially outward. However, the discussion of figure 2(a) appears to suggest that the onset of the spiral arm formation can apparently be located in the more central region of the tank. Although this does not necessarily exclude the spiral arm formation being at least partly due to such a set of roll vortices, there are several other experimental observations which should be considered in the attempt to understand the formation processes.

First is the finding that the stability boundary of the Class B waves approximately coincides with the boundary for spiral arm formation. Second is the result expressed in (8b) that $\lambda(r) \propto \omega_1^{-0.5}$ for $r = \text{const.}$ with $r_0 < r \lesssim R$, which apparently indicates the influence of the Class B instability on the formation process. This would then suggest that the modulation of the flow velocity on the bottom of the tank due to the roll vortices of this class of instability is an important factor in the formation process of the spiral arms. Indeed the video recordings have shown that it is in the troughs of the small-scale pattern pertaining to the roll vortices of the Class B instability where, shortly after the granule motion has been initiated, the first indication of the spiral arm formation process becomes apparent. It can be observed that the first indication of an onset of the pattern formation is that in some apparently random locations the salt bed in these troughs is broken up. This creates spots which are cleared of all salt granules and these spots are initially orientated according to the spiralling direction of the roll vortices at an angle of $\epsilon \approx 15^\circ$ with respect to the tangential direction. However, the video recordings also show that as soon as such a spot is created the angle ϵ starts to grow and the spot thus orientates itself in a more radial direction while apparently growing in size and at times connecting to other such spots. The orientation of the

Class B roll vortices itself is not affected by this as the traces left by these vortices remain unchanged in the areas where salt granules are still present.

However, the roll vortices of the Class B instability on their own are not sufficient to explain the large-scale spiral arm formation as such. Several test runs of the experiment were conducted in which the salt granules were not distributed uniformly across the entire bottom of the tank. Instead they were initially confined to a circular area in the centre of the tank whose radius was chosen to be somewhat larger than the radius of the inner salt patch as predicted by (6). The video recordings, especially the recordings of the test runs of the experiment, indicate that the large-scale spiral arms mainly grow from the central areas of the tank outward, with additional salt granules being deposited preferentially at the radially outermost portion of each of the growing spiral arms (compare figure 2*a*). It thus seems that, as far as the initially resting granules are concerned, the primary influence of the Class B instability is to lead to areas on the bottom of the tank where granule motion is more likely to be initiated or to be sustained than at other locations. However, once the motion of the granules has been initiated, further conditions with respect to the balance of all the forces acting on each granule will have to be accounted for. A possible starting point for a scenario explaining the spiral arm formation could thus be as follows.

The described modulation of the fluid velocity leads to spots near the boundary of the inner salt patch where granules preferentially accumulate. While this happens the boundary of the inner salt patch, at which the action of all factors involved in the reorganization process is just sufficient to initiate granule motion, is simultaneously moved slightly further radially outwards due to the action of the viscosity of the fluid. Hence, granules which have been deposited closer to the centre than the new critical radius are unlikely to be washed away again, thus giving rise to a continuous growth of the spiral arms. Nevertheless, this model would not make any prediction with respect to the number of spiral arms that will be formed. This number is likely to be determined by the balance of the action of all the relevant contributing forces and this appears to be reflected in the final result of (16). The exact scenario of the spiral arm formation at its lowest level of description must be a very complicated interaction of many factors which, however, leads to a simple large-scale structure. In order to understand the formation process starting from the lowest levels one would, for instance, also have to consider the disturbance of the basic flow on the bottom of the tank due to the granule motion itself. During the reorganization process the spacing between the individual granules is of the order of the granules and, moreover, each of the granules carries with it some fluid which surrounds it and as such gives rise to a disturbance of the basic flow. This might then cause some type of feedback mechanism to be set into action, as is for instance often the case in systems displaying a self-organizing behaviour (Anderson 1990). A feedback mechanism that supports the large-scale spiral arm formation might then be responsible for the emerging simple large-scale pattern.

It has been seen that the pattern formation of the salt granules is closely associated with the instability of the boundary layer on the bottom of the tank. However, at this stage there appears to be no obvious and conclusive mechanism which on its own provides a simple means to give at least a qualitative account of the pattern formation process observed and the physical mechanisms involved in it. It has been pointed out where the Class B waves apparently influence the pattern formation process (see (8)) but this result could not explain the pattern as such. Considering the complexity of the interaction of the factors present during the pattern formation process, which are at least the shear stresses, the centrifugal force, the Coriolis force, and the granule

interaction which, due to the fluid carried along by each moving granule, possibly leads to the initiation of some feedback mechanism, the final result (equation (16)) obtained for the number of large-scale spiral arms appears to be a remarkably simple one.

I would like to thank Professor G. I. Barenblatt and Professor G. K. Batchelor for some fruitful discussions, and moreover, Professor G. K. Batchelor for commenting on a draft of the manuscript at a later stage of its preparation.

REFERENCES

- ANDERSON, R. S. 1990 Eolian ripples as examples of self-organization in geomorphological systems. *Earth-Sci. Rev.* **29**, 77–96.
- CALDWELL, D. R. & VAN ATTA, C. W. 1970 Characteristics of Ekman boundary layer instabilities. *J. Fluid Mech.* **44**, 79–95.
- FALLER, A. J. 1963 An experimental study of the instability of the laminar Ekman boundary layer. *J. Fluid Mech.* **15**, 560–576.
- FALLER, A. J. & KAYLOR, R. E. 1965 Investigations of stability and transition in rotating boundary layers. *Tech. Note BN-427*. Institute for Fluid Dynamics and Applied Mathematics, University of Maryland, USA.
- FALLER, A. J. & KAYLOR, R. E. 1966 A numerical study of the instability of the laminar Ekman boundary layer. *J. Atmos. Res.* **23**, 481–494.
- FALLER, A. J. & KAYLOR, R. 1967 Instability of the Ekman spiral with applications to the planetary boundary layers. *Phys. Fluids* **10**, S212–S219.
- FEDEROV, B. I., P LAVNIK, G. Z., PROKHOROV, I. V. & ZHUKHOVITSKII, L. G. 1976 Transitional flow conditions on a rotating disk. *J. Engng Phys.* **31**, 1448–1453.
- GREENSPAN, H. P. 1968 *The Theory of Rotating Fluids*. Cambridge University Press.
- GREGORY, N., STUART, J. T. & WALKER, W. S. 1955 On the stability of three-dimensional boundary layers with application to the flow due to a rotating disk. *Phil. Trans. R. Soc. Lond. A* **248**, 155–199.
- KOBAYASHI, R., KOHAMA, Y. & TAKAMADATE, CH. 1980 Spiral vortices in boundary layer transition regime on a rotating disk. *Acta Mech.* **35**, 71–82.
- KOHAMA, Y. 1984 Study on boundary layer transition of a rotating disk. *Acta Mech.* **50**, 193–199.
- KOHAMA, Y. 1987 Crossflow instability in rotating disk boundary layer. *AIAA Paper* 87-1340.
- MALIK, M. R., WILKINSON, S. P. & ORSZAG, S. A. 1981 Instability and transition in rotating disk flow. *AIAA J.* **19**, 1131–1138.
- OWEN, P. R. 1980 The physics of sand movement. *Lecture Notes of Lectures held at the International Centre for Theoretical Physics, Autumn course on Physics of flow in the oceans, atmosphere and deserts, Trieste, Italy, 30 September–28 November, 1980*.
- REED, H. L. & SARIC, W. S. 1989 Stability of three-dimensional boundary layers. *Ann. Rev. Fluid Mech.* **21**, 235–284.
- TATRO, P. R. & MOLLÖ-CHRISTENSEN, E. L. 1967 Experiments on Ekman layer instability. *J. Fluid Mech.* **28**, 531–543.
- WEAST, R. C. (ed.) 1971 *CRC Handbook of Chemistry and Physics*. The Chemical Rubber Co.
- WILKINSON, S. P. & MALIK, M. R. 1985 Stability experiments in the flow over a rotating disk. *AIAA J.* **23**, 588–595.